JSHC
Japan Society of
Histochemistry and Cytochemistry
Established 1959

Acta Histochem. Cytochem. 49 (4): 117–123, 2016
doi: 10.1267/ahc.16016

Visualization of Neutrophil Extracellular Traps and Fibrin Meshwork in Human Fibrinopurulent Inflammatory Lesions: II. Ultrastructural Study

Takanori Onouchi[1], Kazuya Shiogama[1], Takahiro Matsui[2], Yasuyoshi Mizutani[1], Kouhei Sakurai[3], Ken-ichi Inada[3] and Yutaka Tsutsumi[1]

[1]Department of Pathology, Fujita Health University School of Medicine, Toyoake, Japan, [2]Laboratory Medicine, Toyota Kosei Hospital, Toyota, Japan and [3]Department of Diagnostic Pathology, Banbuntane-Houtokukai Hospital, Fujita Health University School of Medicine, Nagoya, Japan

Received May 7, 2016; accepted June 17, 2016; published online July 30, 2016

Neutrophil extracellular traps (NETs) represent an extracellular, spider's web-like structure resulting from cell death of neutrophils. NETs play an important role in innate immunity against microbial infection, but their roles in human pathological processes remain largely unknown. NETs and fibrin meshwork both showing fibrillar structures are observed at the site of fibrinopurulent inflammation, as described in our sister paper [*Acta Histochem. Cytochem.* 49; 109–116, 2016]. In the present study, immunoelectron microscopic study was performed for visualizing NETs and fibrin fibrils (thick fibrils in our tongue) in formalin-fixed, paraffin-embedded sections of autopsied lung tissue of legionnaire's pneumonia. Lactoferrin and fibrinogen gamma chain were utilized as markers of NETs and fibrin, respectively. Analysis of immuno-scanning electron microscopy indicated that NETs constructed thin fibrils and granular materials were attached onto the NETs fibrils. The smooth-surfaced fibrin fibrils were much thicker than the NETs fibrils. Pre-embedding immunoelectron microscopy demonstrated that lactoferrin immunoreactivities were visible as dots on the fibrils, whereas fibrinogen gamma chain immunoreactivities were homogeneously observed throughout the fibrils. Usefulness of immunoelectron microscopic analysis of NETs and fibrin fibrils should be emphasized.

Key words: neutrophil extracellular traps, fibrin, lactoferrin, fibrinogen gamma chain, immunoelectron microscopy

I. Introduction

A new mechanism for bacterial clearance by neutrophil extracellular traps (NETs) has been reported [2]. NETs are extracellular spider's web-like structures, resulting from cell death of neutrophils [2]. NETs kill gram-positive and gram-negative bacteria extracellularly [2, 10], prevent them from spreading and colonizing new host surfaces [23], and ensure a high local concentration of antimicrobial agents able to degrade virulence factors [10]. The structural component of NETs includes DNA stretches, histones and neutrophil granule-derived antimicrobial proteins, such as neutrophil elastase, myeloperoxidase, cathepsin G, lactoferrin (LF), and gelatinase [2, 19, 26]. Reportedly, hypercitrullination of histone H3 plays an important role in chromatin decondensation in an early stage of NETs formation [13].

NETs carry a protective role by virtue of their property to entrap microbes, but inappropriate NETs release may cause tissue damage and inflammation [5]. Proteins components of NETs accompany a detrimental impact on adjacent tissue function, as suggested in cystic fibrosis [16], transfusion-related acute lung injury [4], asthma [8], and acute respiratory distress syndrome [18]. The NETs-related pathology and clinical implications of NETs remain to be addressed in future studies. The structure of NETs has been analyzed *in vitro* using light microscopy and electron microscopy [2, 10, 16, 26], whereas the *in vivo* analysis of

Correspondence to: Yutaka Tsutsumi, M.D., Department of Pathology, Fujita Health University School of Medicine, Toyoake, Aichi 470–1192, Japan. E-mail: tsutsumi@fujita-hu.ac.jp

NETs is still poor.

It is highly expected that NETs are formed in exudative inflammatory lesions showing fibrinopurulent inflammation, and that fibrin meshwork co-exists with NETs. Fibrin plays an important role in the coagulation process where they are involved in the maintenance of hemostasis [12]. Fibrinogen is cleaved by thrombin to form fibrin, the most abundant component of blood clots, and fibrinogen gamma chain (FGG) is the gamma component of fibrinogen [9]. In the microscopic analysis of NETs structure *in vivo*, distinction between NETs and fibrin is required. LF, a representative iron-containing antimicrobial protein of neutrophil granules [24], can bind to DNA through its positively charged *N*-terminal region, so that the LF-DNA complex is formed on NETs, with anti-microbial activity of LF maintained [14, 24]. LF bound onto the extruded DNA may thus serve as a marker of NETs fibrils.

The aim of the present study was to visualize and identify NETs and fibrin fibrils by electron microscopy. Our sister paper described that LF served as a reliable marker of NETs, and LF positivity often co-existed with fibrin, demonstrated as FGG immunoreactivity [20]. We investigated herein the ultrastructural distribution and localization of LF and FGG in the formalin-fixed, paraffin-embedded sections of autopsied lung tissue of legionnaire's pneumonia, rich in "thick fibrils" of our definition [20]. Immunoelectron microscopy was applied to distinguishing both types of fibrillar components.

II. Materials and Methods

Sample

A lung tissue of legionnaire's pneumonia was obtained at autopsy in Fujita Health University Hospital, Toyoake, Japan. The fresh lung tissue was cut to confirm the presence of lobar pneumonia, and then routinely fixed in 10% formalin and embedded in paraffin wax. In the present study, we focused to analyze the area of fibrinopurulent inflammation accompanying deposition of spider's web-like structures, which were confirmed with hematoxylin-eosin (HE) staining. Thick fibrils of our definition [20] were the target of the present study.

Immunoperoxidase staining

Paraffin sections at 3 μm thickness were mounted on coated glass slides New Silane II (Muto Pure Chemicals, Tokyo, Japan), deparaffinized with xylene, and rehydrated through graded ethanol. For amino acid polymer immunohistochemical staining, endogenous peroxidase activity was quenched with 0.3% hydrogen peroxide in methanol for 30 min at room temperature. After a brief dip in tap water, sections were heat-treated using a pressure pan cooker (Delicio 6L, T-FAL, Rumily, France) in 10 mmol/L citrate buffer, pH 6.0, for 10 min, and left for 30 min at room temperature for cooling. A phosphate-buffered saline (PBS) rinse was interposed between every step. Anti-LF rabbit polyclonal antibody (diluted at 1:300, GenWay Biotech, San Diego, CA, USA) and anti-FGG mouse monoclonal antibody (clone: 1F2, diluted at 1:300, Abnova, Taipei, Taiwan) were incubated overnight at room temperature. As the second layer reagent, Simple Stain MAX-PO (Nichirei Bioscience, Tokyo, Japan) was incubated for 30 min at room temperature. The reaction products were visualized in 50 mmol/L Tris-HCl buffer, pH 7.6, containing 20 mg/dl diaminobenzidine tetrahydrochloride and 0.006% hydrogen peroxide. Finally, the nuclei were lightly counterstained with Mayer's hematoxylin.

Conventional scanning electron microscopy

Paraffin sections at 20 μm thickness were mounted on the coated glass slides New Silane II (Muto Pure Chemicals), deparaffinized with xylene, and rehydrated through graded ethanol. Sections were post-fixed with 1% osmium tetroxide in PBS for 1 hr at room temperature, dehydrated through a graded ethanol series and tertial-butyl alcohol, and dried in a freeze-drying apparatus (JFD-310, JEOL, Tokyo, Japan). After sputter-coated with gold palladium by JFC-1500 (JEOL), the sections were observed on a scanning electron microscopy (S-4000, Hitachi, Tokyo, Japan).

Immuno-scanning electron microscopy

Paraffin sections at 20 μm thickness were mounted on the coated glass slides New Silane II (Muto Pure Chemicals), deparaffinized with xylene, rehydrated through graded ethanol, heat-treated using a pressure pan cooker in 10 mmol/L citrate buffer, pH 6.0, for 10 min, and left for 30 min at room temperature for cooling. A PBS rinse was interposed between every step. Sections were incubated with the anti-LF rabbit polyclonal antibody (diluted at 1:300) and the anti-FGG mouse monoclonal antibody (clone: 1F2, diluted at 1:300) overnight at room temperature, followed by incubation with 20 nm gold-conjugated goat anti-rabbit IgG (diluted at 1:50, Cytodiagnostics, Burlington, Canada) and 60 nm gold-conjugated goat anti-mouse IgG (diluted at 1:50, Cytodiagnostics) for 1 hr at room temperature. To stabilize the antigen-antibody binding, the sections were subsequently fixed in 2.5% glutaraldehyde in PBS for 30 min at room temperature, and post-fixed in 1% osmium tetroxide in PBS for 30 min at room temperature. Sections were then dehydrated in a graded ethanol series and tertial-butyl alcohol, and dried in a freeze-drying apparatus (JFD-310, JEOL). Finally, the sections were sputter-coated with gold palladium by JFC-1500 (JEOL), and observed on a scanning electron microscopy (S-4000, Hitachi).

Pre-embedding immunoelectron microscopy

Pre-embedding immunoelectron microscopy for visualizing NETs and fibrin fibrils was performed as follows. Paraffin sections at 3 μm thickness were mounted on coated glass slides Thinlayer Advanced Cytology Assay System (TACAS, Medical & Biological Laboratories, Nagoya,

Japan). When heat-induced epitope retrieval is needed, TACAS slides are the most optimal coated glass slides for pre-embedding immunoelectron microscopy [17]. Sections were deparaffinized with xylene, and rehydrated through graded ethanol. After endogenous peroxidase quenching, the sections were heat-treated using the pressure pan cooker in 10 mmol/L citrate buffer, pH 6.0, for 10 min, and left for 30 min at room temperature for cooling. A PBS rinse was interposed between every step. Anti-LF rabbit polyclonal antibody (diluted at 1:300) and anti-FGG mouse monoclonal antibody (clone: 1F2, diluted at 1:300) were incubated overnight at room temperature. The secondary reagent (Simple Stain MAX-PO; Nichirei Bioscience) was incubated for 30 min at room temperature, followed by the diaminobenzidine coloring reaction. The sections were sequentially post-fixed in 1% osmium tetroxide in PBS for 1 hr at room temperature, dehydrated in graded ethanol, and embedded in epoxy resin (EPON812, TAAB, Berkshire, UK) with an inverted gelatin capsule method. The opposite surface of the fully dehydrated stained sections was briefly heated by a burner as the tissue transfer procedure. Ultrathin sections were cut on an ultramicrotome (Ultracut N, Reichert-Nissei, Tokyo, Japan) at 80 nm thickness, put on the copper grid, and observed on a transmission electron microscope (H-7650, Hitachi).

To compare the size of NETs and fibrin fibrils, the diameter of randomly-selected 30 LF-positive fibrils (representing NETs fibrils) and 30 FGG-positive fibrils (representing fibrin fibrils) on the immunostained ultrathin sections was measured.

Statistical analysis

Values were presented as the mean±standard error of the mean. The diameter of LF-positive fibrils and FGG-positive fibrils on the immunostained ultrathin sections was compared with two-tailed Student's t-test. Values of $P<0.05$ were considered to indicate statistical significance.

Ethical issue

Use of human material was approved by the ethical review board for clinical and epidemiological investigations at Fujita Health University, Toyoake (approval number: HM15-583).

III. Results

Light microscopic observation

To examine the distribution of NETs and fibrin fibrils in the lesion of legionnaire's pneumonia, HE staining and immunohistochemical staining were comparatively observed (Fig. 1). The deposition of fibrillar structures was confirmed with HE staining (Fig. 1a, d). NETs fibrils were labeled with LF (Fig. 1b, e), and fibrin fibrils were visualized as FGG immunoreactivity (Fig. 1c, f). NETs and fibrin fibrils co-localized to form a web-like structure, corresponding to the thick fibrils as described in our sister paper [20]. In the light microscopic analysis, no apparent difference in the web-like pattern was noted between NETs and fibrin fibrils, except for LF-labeled neutrophils within the lesion.

Conventional scanning electron microscopic observation

Ultrastructural differences between NETs and fibrin fibrils were evaluated. By conventional scanning electron microscopy (Fig. 2), a number of thin (green arrowheads) and thick (red arrowheads) fibrils were observed in areas with LF and FGG co-localization. Granular materials (arrows) were scattered on the surface of thin fibrils.

Immuno-scanning electron microscopic observation

Next, immuno-scanning electron microscopy was performed. Secondary antibodies were conjugated with different sizes of colloidal-gold particles. Anti-rabbit IgG was labeled with 20 nm particles, and anti-mouse IgG was labeled with 60 nm particles. Figure 3 illustrates that the 20 nm gold particles were seen on the surface of thin fibrils (Fig. 3a, c), and the 60 nm gold particles on the surface of thick fibrils (Fig. 3b, d). The thin fibrils were as thin as the diameter of the 20 nm gold particles. The results of immuno-scanning electron microscopy indicated that thin fibrils represented NETs fibrils, while thick fibrils were composed of fibrin.

Pre-embedding immunoelectron microscopic observation

Using pre-embedding immunoelectron microscopy, we evaluated the width of LF-positive fibrils (representing NETs fibrils) and FGG-positive fibrils (representing fibrin fibrils), and the localization pattern of LF and FGG immunoreactivities on the fibrils (Fig. 4). There was significant difference in fibril size between LF-positive fibrils and FGG-positive fibrils: LF-positive fibrils measured 53±16 nm, while FGG-positive fibrils measured 466±98 nm ($P<0.0001$). LF immunoreactivities (Fig. 4a, c) were visible as dots on the thin fibrils (arrows). FGG immunoreactivity was homogeneously distributed throughout the fibrils (Fig. 4b, d).

IV. Discussion

NETs formation represents a potent antimicrobial mechanism of neutrophils. NETs contain proteins that are able to kill or inhibit pathogens. The antimicrobial proteins include granule-derived neutrophil elastase, myeloperoxidase, cathepsin G, lactoferrin (LF), and gelatinase [2, 19, 26]. *In vivo* roles of NETs have been documented in several pathological conditions, such as acute appendicitis and experimental models of shigellosis and preeclampsia [2, 11]. The importance of NETs in host defense was also suggested in experimental models of necrotizing fasciitis and pneumonia [1, 3]. Fibrin meshwork is commonly deposited in exudative inflammatory lesions [6, 25], and the spider's web-like appearance was shown with scanning electron

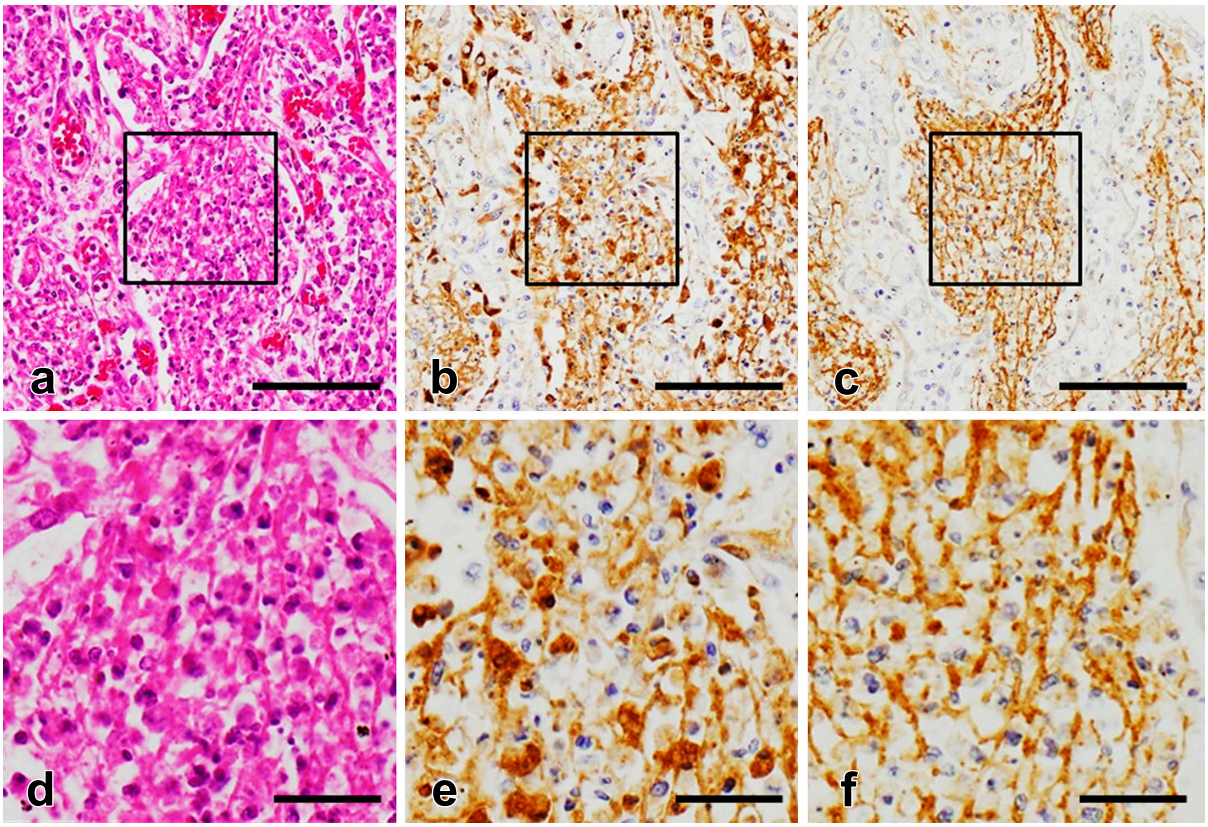

Fig. 1. Immunoreactivities of LF and FGG in legionnaire's pneumonia. Consecutive sections demonstrate (**a, d**) HE-stained features, (**b, e**) LF immunoreactivity representing NETs fibrils, and (**c, f**) FGG immunoreactivity representing fibrin fibrils. Panels (**d–f**) are enlarged images of the squared areas in panels (**a–c**), respectively. "Thick fibrils" of our definition [20] are shown. Bars=100 μm (**a–c**) and 30 μm (**d–f**).

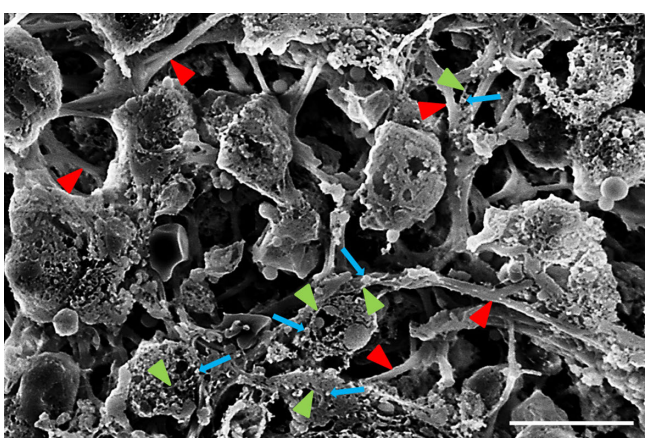

Fig. 2. Conventional scanning electron microscopic observation of thin and thick fibrils in legionnaire's pneumonia. Light green arrowheads indicate thin fibrils, whereas red arrowheads demonstrate thick fibrils. Granular materials on the thin fibrils are shown by blue arrows. Bar=10 μm.

microscopy [22].

Reportedly, when sample shrinkage due to dehydration was considered, the fibril diameter should not be used as a criterion for distinguishing NETs from the fibrin web-like ultrastructure [15]. To challenge this issue, we dared to choose the area accompanying mixed deposition of NETs and fibrin within the same focus of legionnaire's pneumonia as the target of electron microscopic observation. NETs and fibrin fibrils were co-deposited to form a web-like fibrillar structure. Light microscopically, there was little morphologic difference between NETs and fibrin fibrils. However, NETs fibrils showed unique ultrastructural features. It has been reported that a NETs fibril is formed by chromatin filaments of 15 to 17 nm diameter [2], consisting of modified nucleosomes [21], and that they are studded with globular domains of proteins with a diameter up to 50 nm [2]. By scanning electron microscopy, granular materials were often attached on the surface of NETs fibrils, whereas thick fibrin fibrils were smooth-surfaced. Immunoscanning electron microscopy was performed using secondary antibodies conjugated with two different sized colloidal-gold particles. NETs fibrils were labeled with 20 nm-sized particles corresponding to LF immunoreactivity, and fibrin fibrils were decorated with the 60 nm particles corresponding to FGG immunoreactivity. NETs fibrils were as thin as the 20 nm gold particle. Pre-embedding immunoelectron microscopy also distinguished the thin LF-positive fibrils from the thick FGG-positive fibrils. LF-

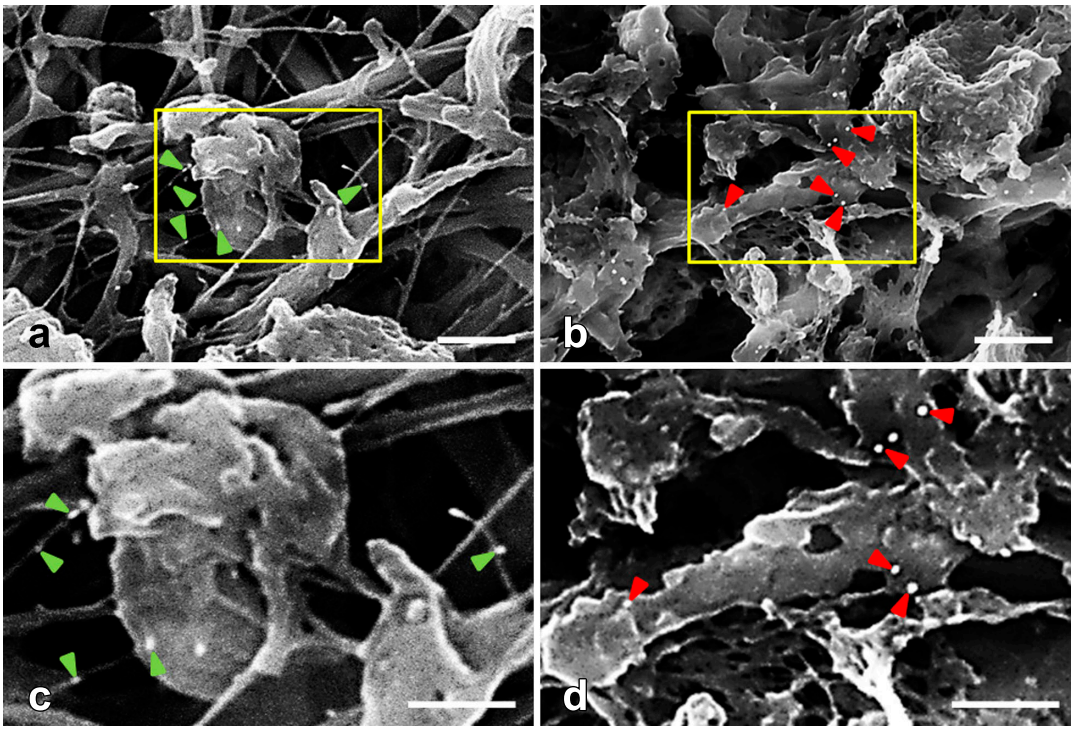

Fig. 3. Immuno-scanning electron microscopy for LF and FGG in legionnaire's pneumonia. (**a, c**) 20 nm immunogold particles (green arrowheads) label LF immunoreactivity on the surface of the thin fibrils. (**b, d**) 60 nm immunogold particles (red arrowheads) label FGG immunoreactivity on the surface of the thick fibrils. Panels (**c, d**) are enlarged images of the squared areas in panels (**a, b**), respectively. Bars=1 μm (**a**), 2 μm (**b**), 250 nm (**c**) and 500 nm (**d**).

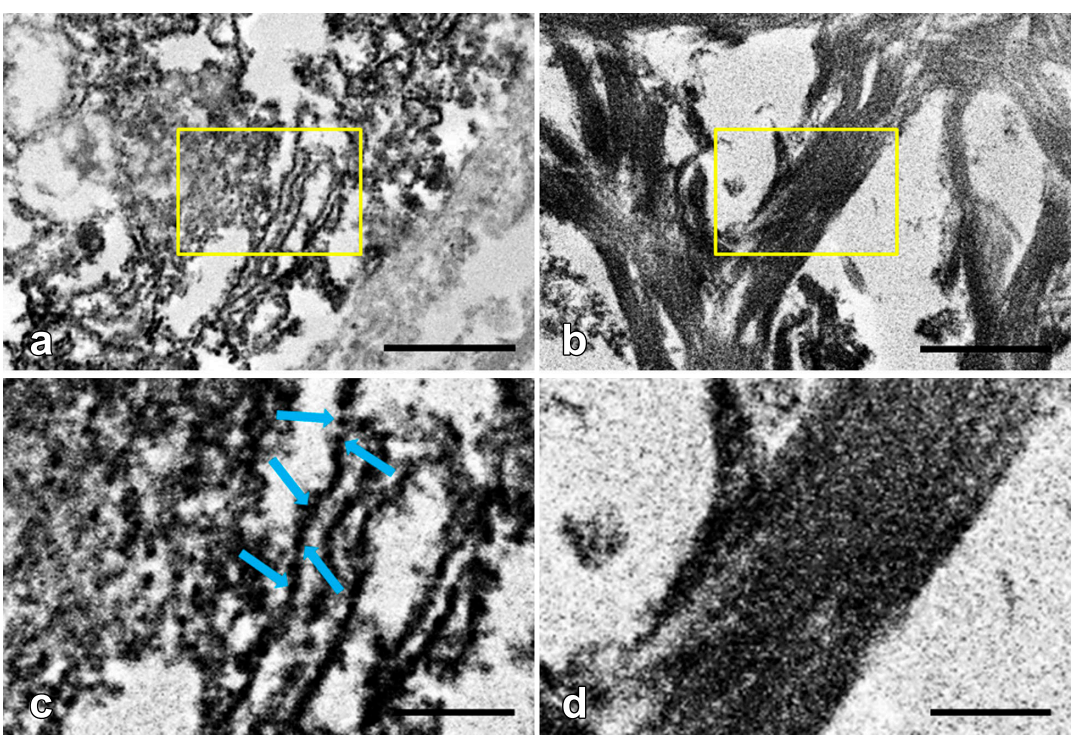

Fig. 4. Pre-embedding immunoelectron microscopy for LF and FGG in legionnaire's pneumonia. LF (**a, c**) and FGG (**b, d**) are labeled with the diaminobenzidine product intensified by osmium black. Panels (**c, d**) are enlarged images of the squared areas in panels (**a, b**), respectively. Blue arrows indicate LF-positive granular materials along the thin fibrils. Bars=1 μm (**a, b**) and 300 nm (**c, d**).

positive fibrils dotted with LF-positive globular structures measured 53±16 nm in width, while FGG-positive fibrils measured 466±98 nm (P<0.0001). The diameter of fibrin frameworks was consistent with the previous reports, describing them as filaments sized 35 to 480 nm [7, 15, 22].

Actually, the diameter of the thick fibrils at the light microscopic level appeared much thicker than that at the electron microscopic level. The discrepancy can be explained as follows. The fibril at the light microscopic level represents a fascicle composed of fine fibrillar components. The detailed observation results will be reported in a separate paper, employing the correlative light and electron microscopy (CLEM) technique.

The present study is the first report demonstrating the ultrastructure of NETs and fibrin fibrils (thick fibrils in our tongue [20]) in routinely prepared paraffin sections. It is of note that formalin-fixed, paraffin-embedded sections were applicable to the immunoelectron microscopic analysis. Archival pathology materials under varied inflammatory/exudative conditions can thus be analyzed for the fine morphology of NETs and fibrin meshwork.

V. Competing Interest Statement

We have no conflict of interest to be claimed.

VI. Acknowledgments

We are grateful to Senior Assistant Prof. Gen Niimi, Ph.D. and Assistant Prof. Tomihiko Ide, Ph.D., Division of Electron Microscopy, Institute of Joint Research, Fujita Health University, Toyoake, Aichi, Japan, for their skillful technical assistance. Ms. Yukika Hasegawa, Ms. Sayaka Takeuchi, Ms. Mika Maeshima, and Ms. Chikayo Yashiro, Department of Pathology, Fujita Health University School of Medicine, Toyoake, are cordially acknowledged for their positive cooperation in our research activity. This work was supported by a Research Grant from Fujita Health University, 2015 (no specific grant number given).

VII. References

1. Beiter, K., Wartha, F., Albiger, B., Normark, S., Zychlinsky, A. and Henriques-Normark, B. (2006) An endonuclease allows Streptococcus pneumoniae to escape from neutrophil extracellular traps. *Curr. Biol.* 16; 401–407.
2. Brinkmann, V., Reichard, U., Goosmann, C., Fauler, B., Uhlemann, Y., Weiss, D. S., Weinrauch, Y. and Zychlinsky, A. (2004) Neutrophil extracellular traps kill bacteria. *Science* 303; 1532–1535.
3. Buchanan, J. T., Simpson, A. J., Aziz, R. K., Liu, G. Y., Kristian, S. A., Kotb, M., Feramisco, J. and Nizet, V. (2006) DNase expression allows the pathogen group A Streptococcus to escape killing in neutrophil extracellular traps. *Curr. Biol.* 16; 396–400.
4. Caudrillier, A., Kessenbrock, K., Gilliss, B. M., Nguyen, J. X., Marques, M. B., Monestier, M., Toy, P., Werb, Z. and Looney, M. R. (2012) Platelets induce neutrophil extracellular traps in transfusion-related acute lung injury. *J. Clin. Invest.* 122; 2661–2671.
5. Cheng, O. Z. and Palaniyar, N. (2013) NET balancing: a problem in inflammatory lung diseases. *Front Immunol.* 4; 1.
6. Chung, C. L., Chen, Y. C. and Chang, S. C. (2003) Effect of repeated thoracenteses on fluid characteristics, cytokines, and fibrinolytic activity in malignant pleural effusion. *Chest* 123; 1188–1195.
7. Collet, J. P., Park, D., Lesty, C., Soria, J., Soria, C., Montalescot, G. and Weisel, J. W. (2000) Influence of fibrin network conformation and fibrin fiber diameter on fibrinolysis speed: dynamic and structural approaches by confocal microscopy. *Arterioscler. Thromb. Vasc. Biol.* 20; 1354–1361.
8. Dworski, R., Simon, H. U., Hoskins, A. and Yousefi, S. (2011) Eosinophil and neutrophil extracellular DNA traps in human allergic asthmatic airways. *J. Allergy Clin. Immunol.* 127; 1260–1266.
9. Farrell, D. H. (2004) Pathophysiologic roles of the fibrinogen gamma chain. *Curr. Opin. Hematol.* 11; 151–155.
10. Fuchs, T. A., Abed, U., Goosmann, C., Hurwitz, R., Schulze, I., Wahn, V., Weinrauch, Y., Brinkmann, V. and Zychlinsky, A. (2007) Novel cell death program leads to neutrophil extracellular traps. *J. Cell Biol.* 176; 231–241.
11. Gupta, A. K., Hasler, P., Holzgreve, W., Gebhardt, S. and Hahn, S. (2005) Induction of neutrophil extracellular DNA lattices by placental microparticles and IL-8 and their presence in preeclampsia. *Hum. Immunol.* 66; 1146–1154.
12. Herd, C. M. and Page, C. P. (1994) Pulmonary immune cells in health and disease: platelets. *Eur. Respir. J.* 7; 1145–1160.
13. Hirose, T., Hamaguchi, S., Matsumoto, N., Irisawa, T., Seki, M., Tasaki, O., Hosotsubo, H., Yamamoto, N., Yamamoto, K., Akeda, Y., Oishi, K., Tomono, K. and Shimazu, T. (2014) Presence of neutrophil extracellular traps and citrullinated histone H3 in the bloodstream of critically ill patients. *PLoS One* 9; e111755.
14. Kanyshkova, T. G., Semenov, D. V., Buneva, V. N. and Nevinsky, G. A. (1999) Human milk lactoferrin binds two DNA molecules with different affinities. *FEBS Lett.* 451; 235–237.
15. Krautgartner, W. D., Klappacher, M., Hannig, M., Obermayer, A., Hartl, D., Marcos, V. and Vitkov, L. (2010) Fibrin mimics neutrophil extracellular traps in SEM. *Ultrastruct. Pathol.* 34; 226–231.
16. Manzenreiter, R., Kienberger, F., Marcos, V., Schilcher, K., Krautgartner, W. D., Obermayer, A., Huml, M., Stoiber, W., Hector, A., Griese, M., Hannig, M., Studnicka, M., Vitkov, L. and Hartl, D. (2012) Ultrastructural characterization of cystic fibrosis sputum using atomic force and scanning electron microscopy. *J. Cyst. Fibros.* 11; 84–92.
17. Matsui, T., Onouchi, T., Shiogama, K., Mizutani, Y., Inada, K., Yu, F., Hayasaka, D., Morita, K., Ogawa, H., Mahara, F. and Tsutsumi, Y. (2015) Coated glass slides TACAS are applicable to heat-assisted immunostaining and in situ hybridization at the electron microscopy level. *Acta Histochem. Cytochem.* 48; 153–157.
18. Narasaraju, T., Yang, E., Samy, R. P., Ng, H. H., Poh, W. P., Liew, A. A., Phoon, M. C., van Rooijen, N. and Chow, V. T. (2011) Excessive neutrophils and neutrophil extracellular traps contribute to acute lung injury of influenza pneumonitis. *Am. J. Pathol.* 179; 199–210.
19. Papayannopoulos, V. and Zychlinsky, A. (2009) NETs: a new strategy for using old weapons. *Trends Immunol.* 30; 513–521.
20. Shiogama, K., Onouchi, T., Mizutani, Y., Sakurai, K., Inada, K. and Tsutsumi, Y. (2016) Visualization of neutrophil extracellular traps and fibrin meshwork in human fibrinopurulent inflammatory lesions: I. Light microscopic study. *Acta Histochem. Cytochem.* 49; 109–116.
21. Urban, C. F., Ermert, D., Schmid, M., Abu-Abed, U., Goosmann, C., Nacken, W., Brinkmann, V., Jungblut, P. R. and Zychlinsky,

A. (2009) Neutrophil extracellular traps contain calprotectin, a cytosolic protein complex involved in host defense against Candida albicans. *PLoS Pathog.* 5; e1000639.
22. Veklich, Y., Francis, C. W., White, J. and Weisel, J. W. (1998) Structural studies of fibrinolysis by electron microscopy. *Blood* 92; 4721–4729.
23. Vitkov, L., Klappacher, M., Hannig, M. and Krautgartner, W. D. (2009) Extracellular neutrophil traps in periodontitis. *J. Periodontal Res.* 44; 664–672.
24. Vogel, H. J. (2012) Lactoferrin, a bird's eye view. *Biochem. Cell Biol.* 90; 233–244.
25. Wait, M. A., Sharma, S., Hohn, J. and Dal Nogare, A. (1997) A randomized trial of empyema therapy. *Chest* 111; 1548–1551.
26. Wartha, F., Beiter, K., Normark, S. and Henriques-Normark, B. (2007) Neutrophil extracellular traps: casting the NET over pathogenesis. *Curr. Opin. Microbiol.* 10; 52–56.